ISTITUTO NAZIONALE DI FISICA NUCLEARE

Sezione di Milano

INFN/AE-96/24
30 Luglio 1996

G. Battistoni, C. Forti, J. Ranft, S. Roesler:

DEVIATIONS FROM THE SUPERPOSITION MODEL IN A DUAL PARTON MODEL APPLIED TO COSMIC RAY INTERACTIONS WITH FORMATION ZONE CASCADE IN BOTH PROJECTILE AND TARGET NUCLEI

PACS: 96.40.Pq, 96.40.Tv, 13.85.Hd, 13.85.Ni, 13.85.Tp

SIS-Pubblicazioni
dei Laboratori Nazionali di Frascati

INFN – Istituto Nazionale di Fisica Nucelare
Sezione di Milano

INFN/AE–96/24
30 Luglio 1996

Deviations from the superposition model in a Dual Parton Model applied to cosmic ray interactions with formation zone cascade in both projectile and target nuclei.

G. Battistoni
INFN, Sezione di Milano, I-20133 Milano, Italy

C. Forti
INFN, Laboratori Nazionali di Frascati, I-00044 Frascati, Italy

J. Ranft
Departamento de Física de Partículas,
Universidade de Santiago de Compostela,
E-15706 Santiago de Compostela, Spain

S. Roesler
Universität Siegen, Fachbereich Physik,D-57068 Siegen, Germany

Abstract

A Dual Parton Model with a formation zone intranuclear cascade in the spectators of the projectile and target nuclei is studied. The hadrons produced in the formation zone cascade contribute to Feynman-x_F and lab-x distributions in the fragmentation regions of the target and projectile nuclei. We discuss the consequences of this model in the secondary cosmic ray production, by analyzing the calculated spectrum weighted moments for pion and kaon production. We show that the proposed model leads to significant differences with respect to a simple superposition model, where the nucleus-nucleus collision is replaced by a few corresponding nucleon-nucleus collisions.

1 Introduction

Nucleus-nucleus collisions are of great importance for understanding the cosmic ray cascade in the atmosphere. Models for sampling hadron production events in nucleus–nucleus and hadron–nucleus collisions are needed for the simulation of the development of cosmic ray showers in atmosphere.

Soft and hard multiple interactions between nucleons of both nuclei dominate the hadron production in most of the kinematic region covered by the interaction and are well described in the framework of the Dual Parton Model (DPM) [1]. They were extensively studied with the Monte Carlo (MC) implementation of this model : DPMJET-II [2]. This event generator was already applied for sampling cosmic ray cascades [2, 3, 4]. However, when dealing with particle or fragment production in the forward or backward fragmentation regions a detailed description of intranuclear cascade processes and of nuclear disintegration is important. A formation zone intranuclear cascade in the target nucleus was therefore considered since a few years [5, 6, 7, 2]. A formation zone intranuclear cascade (FZIC) model in both the target as well as the projectile nucleus, the calculation of nuclear excitation energies, and models for nuclear evaporation, high energy fission and break-up of light nuclei were discussed for hadron–nucleus and nucleus–nucleus collisions in [8, 9]. It was shown that these MC implementations for hadron–nucleus and nucleus–nucleus interactions describe successfully the basic features of target and projectile associated particle production.

The model was compared in [8, 9] mostly to data for asymmetric collisions in which projectile and target masses are different. It seems that the performance of the model in these collisions is rather good. Asymmetric collisions are the most common ones also in cosmic ray cascades.

In Section 2 we summarize briefly the main steps of sampling hadron–nucleus and nucleus–nucleus interactions within the event generator DPMJET-II. Furthermore, we summarize the basic ideas of the FZIC model. In Section 3 we calculate Feynman–x_F distributions of pions produced in hadron–nucleus and nucleus–nucleus collisions. In Section 4 we study spectrum–weighted moments and compare them with the expectations from superposition models. Finally, in Section 5 we summarize our results.

2 The two-component DPM for hadron-nucleus and nucleus-nucleus collisions

2.1 The DPMJET–II event generator

The two-component DPM and its MC realizations for hadron–hadron, hadron–nucleus and nucleus–nucleus collisions have been discussed in detail in [10, 11, 2]. Therefore, we briefly summarize the main steps leading to the multiparticle state, which is the starting point for the intranuclear cascade.

The MC model for hadron-nucleus and nucleus-nucleus interactions starts from an impulse approximation for the nucleons of the interacting nuclei. The spatial initial configuration, i.e. the positions of the nucleons in space-time in the rest system of the corresponding nucleus, is sampled from standard density distributions. For energies above 3-5 GeV/nucleon the collision proceeds via ν elementary interactions between ν_p and ν_t nucleons from the projectile and target, respectively. The values ν, ν_p, and ν_t are sampled according to Glauber's multiple scattering formalism using the MC algorithm of [12]. The particle production is well described by the two-component DPM which is applied as in hadron-hadron interactions [10, 11]. As a result, a system of chains connecting partons of the nucleons involved in the scattering process is formed. The chains are hadronized applying the JETSET model [13, 14]. The hadrons may then cause intranuclear cascade processes, which are treated by the FZIC model [5], an extension of the intranuclear cascade model [15, 16]. At energies below 3-5 GeV/nucleon the FZIC model is able by itself to describe reasonably the inelastic nuclear collisions.

2.2 The formation zone cascade in target and projectile nuclei

In the following we summarize the main ideas of the FZIC model for hadron-nucleus and nucleus–nucleus interactions [5, 6, 7, 2, 8, 9]. The physical picture explaining the absence of the intranuclear cascade at high energies is the concept of the formation zone [17]. It has been introduced in analogy to the Landau-Pomeranchuk [18] effect, which explains the observation that electrons passing through high density materials become more penetrating at high energies. For the formation zone of an electron with 4-momentum p and energy E upon radiation of a photon with 4-momentum k one obtains

$$\tau = \frac{E}{k \cdot p} = \frac{E}{m} \frac{1}{\omega_e}, \tag{1}$$

where ω_e is the frequency of the photon in the rest frame of the electron and E/m is the time dilatation factor from the electron rest frame to the laboratory. Within the quark model, the states being formed in the primary nucleon-nucleon interaction can be understood as consisting of valence quarks only, i.e without the full system of sea quarks, antiquarks, and gluons and have therefore a reduced probability for hadronic interactions inside the nucleus [5]. The formation zone concept can be translated to hadron production as follows [6]. We consider the formation zone cascade in the rest system of the target nucleus (laboratory system) or in the rest system of the projectile nucleus. Denoting the 4-momenta of the projectile hadron p_p and of the secondary hadron p_s with

$$p_p = (E_p, 0, 0, \sqrt{E_p^2 - m_p^2}), \qquad p_s = (E_s, \vec{p}_{s\perp}, \sqrt{E_s^2 - m_s^2 - \vec{p}_{s\perp}^2}) \tag{2}$$

and replacing in Eq. (1) the electron momentum by p_p and the photon momentum by p_s, the hadron formation time reads, for $E_p \gg m_p$:

$$\tau_{\rm Lab} = \frac{2E_s}{(m_p x)^2 + m_s^2 + p_{s\perp}^2}, \qquad x = \frac{E_s}{E_p}. \tag{3}$$

The term $(m_p x)^2$ can be neglected for most of the produced secondaries, so one can approximate

$$\tau_{\rm Lab} \approx \gamma_s \tau_s, \qquad \gamma_s = \frac{E_s}{m_s}. \tag{4}$$

We define an average formation time to create a complete hadronic state τ_s in the rest system of the secondary hadron s, [5, 6]

$$\tau_s = \tau_0 \frac{m_s^2}{m_s^2 + p_{s\perp}^2}. \tag{5}$$

τ_0 is a free parameter, which has to be determined by comparing particle production within the model to experimental data. Typical values are in the range from 1 fm/c to 10 fm/c. Here we use $\tau_0 = 4.5$ fm/c. For each secondary we sample a formation time τ from an exponential distribution [19] with an average value as given in Eq. (5). As it was described in [7], in the MC model the full space-time history of the collision is known.

After having assigned a formation time to a secondary, its spatial coordinates in the rest system of both nuclei are known and we start with considering an intranuclear cascade step in one (randomly chosen) of the spectators.

Due to relativistic time dilatation, those secondaries having sufficiently high energies in the rest frame of the considered nucleus are formed mostly outside of the spectator part of this nucleus, whereas those with lower energies are formed inside. The latter may penetrate the spectator and initiate intranuclear cascade processes. Elastic and inelastic interactions with spectator nucleons are treated using the MC-model HADRIN [20]. This code is based on measured cross sections and interaction channels up to a laboratory momentum of 5 GeV. We apply HADRIN to hadron-nucleon interactions up to 9 GeV and neglect those at higher energies. Reinteractions beyond 5 GeV occur much less frequently than reinteractions below 5 GeV and a more detailed treatment would not change the results discussed in this paper. Furthermore, we take into account absorption of low-energy mesons and antiprotons by interactions with two-nucleon systems (for pion absorption we use the cross sections as given by Ritchie [21]) and Pauli's principle [7]. In case no interaction is possible in the considered spectator, we proceed with sampling a cascade step in another spectator.

For secondaries produced in intranuclear cascade processes we apply the same formalism, i.e. a formation time is sampled, the secondary is transported to the end of the formation zone and reinteractions are treated if they are possible. Due

to these intranuclear cascade processes, nucleons are knocked out of the residual spectator nuclei if their energy is high enough to escape from the nuclear potential.

In Ref. [9], it has been stressed that the model with FZIC and the calculation of nuclear excitation energies is expected to work reliably only in peripheral collisions. In a peripheral nucleus-nucleus collision, the spectator part of one of the interacting nuclei looks still like a deformed nucleus and it can be treated as a highly excited nucleus, which subsequently looses its excitation energy by nuclear evaporation, Fermi break–up and emission of gammas. In a central Fe–O collision there are probably no spectators from the O–nucleus and the spectators of the Fe–nucleus are in the shape of the original Fe–nucleus with one hole of cylindrical shape in the center. This system cannot be treated as an excited nucleus; it will probably first fragment into some smaller droplets before the nuclear evaporation and de–excitation start. There is no model for multifragmentation implemented at present in DPMJET–II. It is not correct to treat the Fe–spectator after the central collision just like one excited nucleus which evolves into one residual nucleus. We might conclude that, if we apply the mode to central collisions, the treatments of nuclear evaporation and the formation of a stable residual nucleus become incorrect. Also, the FZIC is a rather fast process, which will not break down completely even in central collisions. In spite of these problems, we apply the model in minimum bias situations to all collisions, since the fraction of central collisions, where it might fail, is rather small. Furthermore, here we are mainly interested in the FZIC component, for which these restrictions are less important.

3 Feynman–x_F distributions in hadron–nucleus and nucleus–nucleus collisions

The so-called "cascade particles" are the particles which are produced or knocked–out off the spectator nucleus by the FZIC. Target associated cascade particles are experimentally studied (in emulsion experiments) and are often called "grey" prongs.

In the papers [8, 9] most of the available data on grey particle production in high energy hadron–nucleus and nucleus–nucleus collisions is compared to the model we use. Reasonable agreement is found as far as the average multiplicities of grey prongs, their multiplicity and angular distribution, and their correlations with the number of fast produced particles are concerned. There are two kinds of particles contributing to the grey prongs: protons and charged pions. The emulsion experiments are not able to differentiate between such protons and charged pions. There is however one heavy ion experiment (WA80 [22, 23]), which presents only protons in the energy region of the grey prongs in their multiplicity distributions. We can only draw some rather indirect support for the ability of our model to describe the pions from the intranuclear cascade, from the fact that the model agrees as well to the emulsion data on grey prongs as to the WA80 data on protons alone. Roughly 20% of the grey

prongs (defined with Lorentz parameter $0.23 < \beta < 0.70$) in the model are charged pions[9].

The Feynman–x_F distributions are the most suitable way to present the particle production in the target and projectile fragmentation regions. Unfortunately, most experiments, which measure grey prongs are not able to measure the particle momenta and identity and are therefore not able to present Feynman–x_F distributions. We define Feynman–x_F in h–A and A–A collisions with the longitudinal momentum in the hadron-nucleon (or nucleon-nucleon) cms p_z^{cms} :

$$x_F = \frac{p_z^{cms}}{|p_{z,max}^{cms}|} \tag{6}$$

where we use a $p_{z,max}^{cms}$ calculated disregarding Fermi momenta. The Feynman–x_F distribution $f(x_F)$ is defined as follows

$$f(x_F) = x_F \frac{dN}{dx_F}. \tag{7}$$

For cosmic ray calculations, we are mainly interested in the contributions of pions from the intranuclear cascade to the Feynman–x_F distributions in the fragmentation region of the projectile nucleus, since particles from target fragmentation are very slow in the lab–frame. However, experimental data about the target fragmentation are very important for the tuning of the interaction model. The changes in Feynman–x_F distributions from p–p to p–nucleus collisions in the proton fragmentation region have been measured (and have been compared to DPMJET–II in [2]), but we are not aware of any such measurements in the fragmentation region of the nucleus. Therefore, we have to rely on the model, but we stress that it would be highly desirable to measure Feynman–x_F distributions in the fragmentation region of target or projectile nuclei.

In Fig. 1 we present the Feynman–x_F distribution of π^+ mesons in p–air collisions at a lab–energy of 500 TeV . There are two plots, one for the full model with formation zone intranuclear cascade in the target nucleus, and one without this cascade. We also compare the distributions with the one in p–p collisions at the same energy. In the target fragmentation region, at x_F values between -0.3 and -1 we find significant differences in the distributions due to the pions produced by the formation zone cascade in the target nucleus. The difference between both plots is not due to a large number of particles. If we define "grey" the particles with Lorentz–β of $0.23 < \beta < 0.70$ in the lab–frame, we find in the calculation 0.06 grey π^+ per interaction, on average. However, not all charged pions from the formation zone cascade belong to the grey particles.

Next we turn to nucleus–air collisions and calculate again Feynman–x_F distributions. For our later discussion, we note that the Feynman–x_F distribution at positive x_F in the projectile fragmentation region is a very good approximation to the x_{lab} distribution.

In Figs. 2 to 5 we present the Feynman–x_F distribution of π^+ mesons at a lab–energy of 500 TeV per projectile nucleon in He–air, O–air, Si–air, and Fe–air collisions. The model, as was shown in [2], has a rather good Feynman–scaling behaviour, so that these distributions look rather similar also at other different energies. Fig.2 is included mainly to demonstrate, that for a light nucleus like He the formation zone cascade really makes no difference and could be neglected. There are on each figure two plots, one for the full model with formation zone intranuclear cascade in the target as well as in the projectile nucleus and one without this cascade. We also compare the distributions with the corresponding in p–air collisions at the same energy and with the formation zone cascade. In the target fragmentation region, at x_F values between -0.3 and -1 we find in each plot nearly the same differences in the distributions due to the pions produced by the formation zone cascade in the target nucleus. Such differences are also visible in the projectile fragmentation region at positive x_F values, but here those differences, which are not significant in the case of He–air collisions (there is nearly no cascade in the spectators of the He nucleus), rise with the mass number of the projectile nucleus. Clearly, the formation zone cascade in the spectators of the Fe nucleus produces more pions than the one in the O–spectators.

We will see in the next section that these hadrons produced by the formation zone cascade lead to significant changes also in the spectrum weighted moments.

4 Spectrum weighted moments and comparison with superposition models

Following for instance the basic discussion of Ref. [24], we introduce a variable x_{lab} similarly to Feynman–x_F, but this time in the lab–frame :

$$x_{lab} = \frac{E_i}{E_0}, \tag{8}$$

E_i is the lab–energy of a secondary particle i and E_0 is the lab–energy of the projectile in a h–A collision (or the energy per projectile nucleon in a A–A collision). We introduce x_{lab} distributions $F(x_{lab})$:

$$F_i(x_{lab}) = x_{lab}\frac{dN}{dx_{lab}}. \tag{9}$$

The spectrum weighted moments in A–B collisions are defined as moments of the $F(x_{lab})$

$$Z_i^{A-B} = \int_0^1 (x_{lab})^{\gamma-1} F_i^{A-B}(x_{lab}) dx_{lab}. \tag{10}$$

Here $-\gamma \simeq -1.7$ is the power of the integral cosmic ray energy spectrum. The spectrum weighted moments determine the uncorrelated fluxes of energetic particles in the atmosphere. After recalling the concept of superposition model, in the following we

shall compare the calculation of spectrum weighted moments with our model in different conditions, pointing out the differences with respect to a simple superposition model.

4.1 The superposition model

Generally, we call superposition model the approximation in which the collision of a nucleus A, with total energy E, against a target B, is treated as the superposition of A independent nucleon-B collisions, each nucleon having an energy E/A. This model is based on the hypothesis that, when the energy per nucleon of the projectile is much larger than the single nucleon binding energy, the A nucleons will interact incoherently. In this context, in cosmic ray simulations, for a primary of total energy E and mass number A (A>1), the cascade generated is equivalent to the total effect of A showers initiated by A independent nucleons of energy E/A. For example, the cascade for a primary iron nucleus of 560 TeV would be simulated as the superposition of 26 proton + 30 neutron initiated showers, each of 10 TeV. Examples of application of the superposition model to cosmic ray calculations can be found in Ref. [25, 26]. The superposition model brings, for instance, to the conclusion that $Z_\pi^{AB} = N_A Z_\pi^{pB}$ (for the same energy/nucleon of the projectile), where N_A is the average number of participating nucleons in the projectile, as resulting from a Glauber calculation.

Among the most relevant effects of this model in the results of calculations for cosmic ray cascades, we mention that :

- the average electromagnetic size $\langle N_e \rangle$ and muon number $\langle N_\mu \rangle$ for primary nuclei of mass A and energy E is A times the corresponding average for primary protons of energy E/A; for example :$\langle N_\mu \rangle$(A,E) = A·$\langle N_\mu \rangle$(1,E/A);

- the average muon lateral displacement $\langle R_\mu \rangle$ (*i.e.* the perpendicular distance from shower axis) depends on mass and energy only through the ratio E/A, that is : $\langle R_\mu \rangle$(A,E) = $\langle R_\mu \rangle$(1,E/A).

One of the main shortcomings of the superposition model comes from the fact that the interaction length of a nuclear projectile is exactly the same as that of a nucleon, at the same energy/nucleon. This results in a biased distribution of interaction heights in the cascade calculations. In order to obtain a more realistic distribution of interaction lengths in the framework of cosmic ray simulations, an alternative approach is the so-called "semi-superposition model" (SSM). As for the "pure" superposition model (PSM) described above, also in the SSM the shower is the result of A independent nucleon showers; however, the distribution of the positions of their first interaction is determined by calculating the successive fragmentation depths, using nucleus–air cross sections and accounting for the properties of the fragmentation of the residual nuclei composed of spectator (non-interacting) nucleons. In this model, the A–air cross sections for all nuclei with mass $\leq$A (all possible fragments) are required, together with a method for the nuclear fragmentation (in particular

to determine the fraction of wounded nucleons, i.e. the nucleons of the projectile directly interacting inside the air target). A first version of this model is described in [27] and applied to high energy muons in [28]. A more recent and accurate version is described in [29], and is applied, for example, in [30, 3] (for the calculation of muons and electromagnetic shower size). In both papers [28] and [3], a comparison with the PSM is reported. Clearly, the semi–superposition is still an approximation with respect to the realistic nuclear interaction, in which we expect a more complex dynamics of the final states.

4.2 Calculation results

In Table 1 and 2 we present spectrum weighted moments as calculated in DPMJET–II in the model with full FZIC and in the model without the FZIC. We consider p–air, He–air, O–air, Si–air, and Fe–air collisions at laboratory energies per nucleon of 50 GeV, 500 TeV, and $5 \cdot 10^6$ TeV, the latter energy ($5 \cdot 10^{18}$ eV) is the absolute highest energy at which DPMJET–II is valid, at present. We also give the number of Glauber collisions ν between ν_p projectile and ν_t target nucleons in minimum bias collisions in Table 1.

The differences between the spectrum weighted moments of the pions in both Tables are easy to understand looking at the previously presented Feynman–x_F distributions in the projectile fragmentation regions.

In Tables 3 and 4 we compare at two energies the spectrum weighted moments of pions and kaons according to the model, with and without FZIC, with the moments obtained from the superposition model. Let us first discuss Table 4. At the upper energy we find a rather perfect agreement of the moments with the superposition model. We have to remember that all numbers are the result of Monte Carlo calculations with typically 5% statistical error. At the lower energy we find that the moments from DPMJET–II are typically 10 to 15% above the moments resulting from the superposition model. This seems surprising. The explanation for this is the diffractive component, which contributes in DPMJET–II to the p–air cross section but not to the nucleus–nucleus cross sections. The single diffractive cross sections in hadron–nucleus collisions are well studied [31, 32] and included in the model. The cross sections for single diffractive nucleus–nucleus collisions are straightforward to calculate within the DPM, and they will probably have a size similar to that obtained in hadron–nucleus collisions. The O–air or Fe-air total cross sections are three to five times larger than the p–air total cross section. Therefore, the fraction of single diffractive nucleus–nucleus collisions will come out to be a few times smaller than in hadron–nucleus collisions. For these reasons, and because of the lack of experimental data on single diffractive nucleus–nucleus cross sections, this component is not included at present in the DPMJET–II event generator (however, the inclusion of this part would probably not change the situation). Now, in the case of diffractive p–air collisions, where the projectile proton leaves the collision only slightly deflected and in which hadrons are produced only in the nucleus fragmentation region, nearly

no contribution to the moments of pions and kaons is achieved. It seems, that this effect, which should also act at the higher energy, is compensated there by a stronger change of the x_{lab} distributions of pions and kaons when going from p–air to nucleus–air collisions.

In summary we may conclude that for the model without formation zone intranuclear cascade we find an agreement with the superposition model within approximately 10%.

Now we turn to Table 3 and compare the results of DPMJET–II with full FZIC with the superposition model. While for He–air collisions the model agrees practically to the model without formation zone cascade, we find that for Fe–air differences are up to 50% from the superposition model. These differences are certainly significant and should also lead to differences when sampling the cosmic ray cascade with the full DPMJET–II model as compared to the sampling using the superposition model. A larger value for Z_π means that, on average, the primary cosmic ray loses a larger fraction of its energy in the first interaction. This energy is spent for pion production. This should probably lead to showers with a larger muon content and with a smaller depth of the maximum development (thus with a smaller electromagnetic size at mountain or sea level). We are still studying the effects of the FZIC model on cosmic ray showers, as a function of the primary energy and mass.

Unfortunately, there is no obvious way to compare spectrum weighted moments or inelasticities of nucleons between the full model and superposition models. We give an example to illustrate this. In collisions at 500 TeV per projectile nucleon we obtain for the spectrum weighted moments of protons $Z_p^{p-air} = 0.124$ and $Z_p^{Fe-air} = 6.40$. With $\nu_p = 11.98$ (see Table 1) we would get $\nu_p Z_p^{p-air} = 1.47$. The reason for these big differences is the particle content in the full DPMJET–II model: it contains, in addition to the nucleons produced in the first step of the calculation, the Glauber cascade, also the nucleons knocked out of the nuclei by the formation zone cascade and evaporation nucleons. But not all spectator nucleons come as cascade nucleons or evaporation nucleons. There are in addition also light fragments from the evaporation step and there is a stable residual nucleus. The conclusion is that only in the restricted model without formation zone cascade and nuclear evaporation it would make sense to compare spectrum weighted moments or inelasticities of nucleons with the results from a superposition model. But what we want to stress here are the results achieved with the full model. We might however conclude that, when simulating the full cosmic ray cascade initiated by primary nuclei, the full model could well show further deviations from the superposition model which are not simply contained in the differences of spectrum weighted moments of pions and kaons. This is another reason to stress the importance of studying the full model in shower simulations.

5 Conclusions and summary

We have compared Feynman–x_F distributions and spectrum weighted moments of pions and kaons in two versions of the two component Dual Parton Model. One version is the full model with FZIC of the produced hadrons with the spectators of the target and projectile nuclei, the second version is the DPM without this formation zone cascade.

We find a reasonable, however not perfect, agreement of the moments from the restricted model for nucleus–nucleus collisions with a superposition model. However, in the full model the hadrons produced in the projectile fragmentation region by the formation zone cascade lead to significant deviations in the pion spectrum weighted moments from the superposition model. For Fe–air collisions this difference becomes as large as 50%. This effect depends on the changes in the Feynman–x_F distributions due to the cascade in the projectile nucleus. We have stressed above that there is no direct experimental evidence for this. Therefore we cannot be completely sure about the quantitative size of the predicted effect, but we are convinced that this effect exists.

On the basis of differences in the calculated spectrum weighted moments of pions (also for the π^0, where the differences are similar) and kaons, we expect that, when sampling cosmic ray cascades using our full model, a higher fraction of energy from the first interactions will go into the electromagnetic component and energetic muons, with respect to the case of a simple superposition model. On the other hand, we expect that less energy is carried away by the leading particles, so that the development of the shower will be different from that resulting from the superposition model. In order to understand the differences in the predictions for ground-based observations, (for instance the electromagnetic size as measured at a fixed depth in the atmosphere), detailed simulations of full showers are necessary.

Acknowledgements One of the authors (J.R.) thanks Professor C.Pajares for the hospitality at Santiago de Compostela and he was supported by the Direccion General de Politicia Cientifica of Spain.

References

[1] A. Capella, U. Sukhatme, C. I. Tan and J. Tran Thanh Van: Phys. Rep. 236 (1994) 227

[2] J. Ranft: Phys. Rev. D51 (1995) 64

[3] G. Battistoni, C. Forti and J. Ranft: Astroparticle Phys. 3 (1995) 157

[4] G. Battistoni, C. Bloise, C. Forti, M. Greco, J. Ranft and A. Tanzini: Astroparticle Physics 4 (1996) 351

[5] J. Ranft: Phys. Rev. D37 (1988) 1842

[6] J. Ranft: Z. Phys. C43 (1989) 439

[7] H.-J. Möhring and J. Ranft: Z. Phys. C52 (1991) 643

[8] A. Ferrari, J. Ranft, S. Roesler and P. R. Sala: Z. Phys. C70 (1996) 413

[9] A. Ferrari, J. Ranft, S. Roesler and P. R. Sala: The production of residual nuclei in peripheral high energy nucleus-nucleus interactions, Santiago US–FT /9–96, 1996

[10] P. Aurenche, F. W. Bopp, A. Capella, J. Kwiecinski, M. Maire, J. Ranft and J. Tran Thanh Van: Phys. Rev. D45 (1992) 92

[11] F. W. Bopp, R. Engel, D. Pertermann and J. Ranft: Phys. Rev. D49 (1994) 3236

[12] S. Y. Shmakov, V. V. Uzhinskii and A. M. Zadoroshny: Comp. Phys. Commun. 54 (1989) 125

[13] T. Sjöstrand: Comp. Phys. Commun. 39 (1986) 347

[14] T. Sjöstrand and M. Bengtsson: Comp. Phys. Commun. 43 (1987) 367

[15] H. W. Bertini: Phys. Rev. 137 (1963) 1801

[16] H. W. Bertini: Phys. Rev. 188 (1969) 1711

[17] L. Stodolski: Proceedings on the Colloquium on Multiparticle Reactions, Oxford (1975) 577

[18] L. Landau and I. Pomeranchuk: Dokl. Akad. Nauk SSR 92 (1953) 535,734

[19] A. Bialas: Z. Phys. C26 (1984) 301

[20] K. Hänssgen and J. Ranft: Comp. Phys. Commun. 39 (1986) 37

[21] B. G. Ritchie: Phys. Rev. C 28 (1983) 926

[22] WA80 Collab.: R. Albrecht et al.: Z. Phys. C57 (1993) 37

[23] WA80 Collab.: R. Albrecht et al.: Phys. Lett. B309 (1993) 269

[24] T. K. Gaisser: *Cosmic Rays and Particle Physics,* Cambridge University Press, 1990

[25] J.W. Elbert, T.K. Gaisser and T. Stanev: Phys. Rev. D27 (1983) 1448

[26] T. K. Gaisser and T. Stanev: Nuclear Instr. & Meth. A235 (1985) 183

[27] T.K. Gaisser, T. Stanev, P. Freier and C.J. Waddington: Phys. Rev. D25 (1982) 2341

[28] C. Forti, H. Bilokon, B. d'Ettorre Piazzoli, T.K. Gaisser, L. Satta and T. Stanev: Phys. Rev. D42 (1990) 3668

[29] J. Engel, T.K. Gaisser, P. Lipari and T. Stanev: Phys. Rev. D46 (1992) 5013

[30] R.S. Fletcher, T.K. Gaisser, P. Lipari and T. Stanev,: Phys. Rev. D50 (1994) 5710

[31] S. Roesler, R. Engel and J. Ranft: Z. Phys. C59 (1993) 481

[32] J. Ranft and S. Roesler: Z. Phys. C62 (1994) 329

Table 1: Spectrum weighted moments of pions and kaons according to DPMJET–II in the model with full FZIC. We give also the values of ν, ν_p and ν_t for the minimum bias Glauber cascade introduced in Section 2.1. E is the lab–energy per projectile nucleon.

Collision	E (TeV)	ν	ν_p	ν_t	Z_π	Z_K
p–air	0.05	1.72	1.	1.72	0.0922	0.00919
	500	2.21	1.	2.21	0.0670	0.00952
	$5 \cdot 10^6$	2.84	1.	2.84	0.0755	0.00936
He–air	0.05	3.05	2.00	2.59	0.212	0.0188
	500	4.43	2.32	3.42	0.176	0.0249
	$5 \cdot 10^6$	6.51	2.57	4.36	0.170	0.0243
O–air	0.05	6.78	4.52	4.37	0.574	0.0536
	500	10.24	5.59	5.32	0.506	0.0636
	$5 \cdot 10^6$	16.55	6.73	6.28	0.539	0.0681
Si–air	0.05	9.63	6.42	5.23	0.803	0.0806
	500	14.43	7.95	6.08	0.764	0.0822
	$5 \cdot 10^6$	22.97	9.59	6.83	0.843	0.1018
Fe–air	0.05	13.89	9.50	6.25	1.355	0.145
	500	21.73	11.98	6.95	1.236	0.143
	$5 \cdot 10^6$	34.34	14.67	7.55	1.382	0.154

Table 2: Spectrum weighted moments of pions and kaons according to DPMJET–II in the model without FZIC. E is the lab–energy per projectile nucleon.

Collision	E (TeV)	Z_π	Z_K
p–air	0.05	0.0882	0.01009
	500	0.0631	0.00943
	$5 \cdot 10^6$	0.0733	0.00881
He–air	0.05	0.211	0.0207
	500	0.176	0.0242
	$5 \cdot 10^6$	0.175	0.0241
O–air	0.05	0.506	0.0506
	500	0.419	0.0589
	$5 \cdot 10^6$	0.459	0.0668
Si–air	0.05	0.690	0.0770
	500	0.625	0.0890
	$5 \cdot 10^6$	0.719	0.0963
Fe–air	0.05	1.015	0.117
	500	0.923	0.121
	$5 \cdot 10^6$	1.056	0.139

Table 3: Spectrum weighted moments of pions and kaons according to DPMJET–II in the model with full FZIC compared with the moments expected in a superposition model. E is the lab–energy per projectile nucleon.

Collision	E (TeV)	ν_p	Z_π	$\nu_p Z_\pi^{p-air}$	Z_K	$\nu_p Z_K^{p-air}$
p–air	500	1.	0.0670		0.00952	
He–air	500	2.32	0.176	0.155	0.0249	0.0221
O–air	500	5.59	0.506	0.375	0.0636	0.0532
Si–air	500	7.95	0.764	0.533	0.0822	0.0757
Fe–air	500	11.98	1.236	0.803	0.143	0.114
p–air	$5 \cdot 10^6$	1.	0.0755		0.00936	
He–air	$5 \cdot 10^6$	2.57	0.170	0.194	0.0243	0.0241
O–air	$5 \cdot 10^6$	6.73	0.539	0.508	0.0681	0.0630
Si–air	$5 \cdot 10^6$	9.59	0.843	0.724	0.102	0.0898
Fe–air	$5 \cdot 10^6$	14.67	1.382	1.108	0.154	0.137

Table 4: Spectrum weighted moments of pions and kaons according to DPMJET–II in the model without FZIC compared with the moments expected in a superposition model. E is the lab–energy per projectile nucleon.

Collision	E (TeV)	ν_p	Z_π	$\nu_p Z_\pi^{p-air}$	Z_K	$\nu_p Z_K^{p-air}$
p–air	500	1.	0.0631		0.00943	
He–air	500	2.32	0.176	0.146	0.0242	0.0219
O–air	500	5.59	0.419	0.353	0.0589	0.0527
Si–air	500	7.95	0.625	0.502	0.0890	0.0750
Fe–air	500	11.98	0.923	0.756	0.121	0.113
p–air	$5 \cdot 10^6$	1.	0.0733		0.00881	
He–air	$5 \cdot 10^6$	2.57	0.175	0.188	0.0241	0.0226
O–air	$5 \cdot 10^6$	6.73	0.459	0.493	0.0668	0.0593
Si–air	$5 \cdot 10^6$	9.59	0.719	0.703	0.0961	0.0845
Fe–air	$5 \cdot 10^6$	14.67	1.056	1.075	0.139	0.129

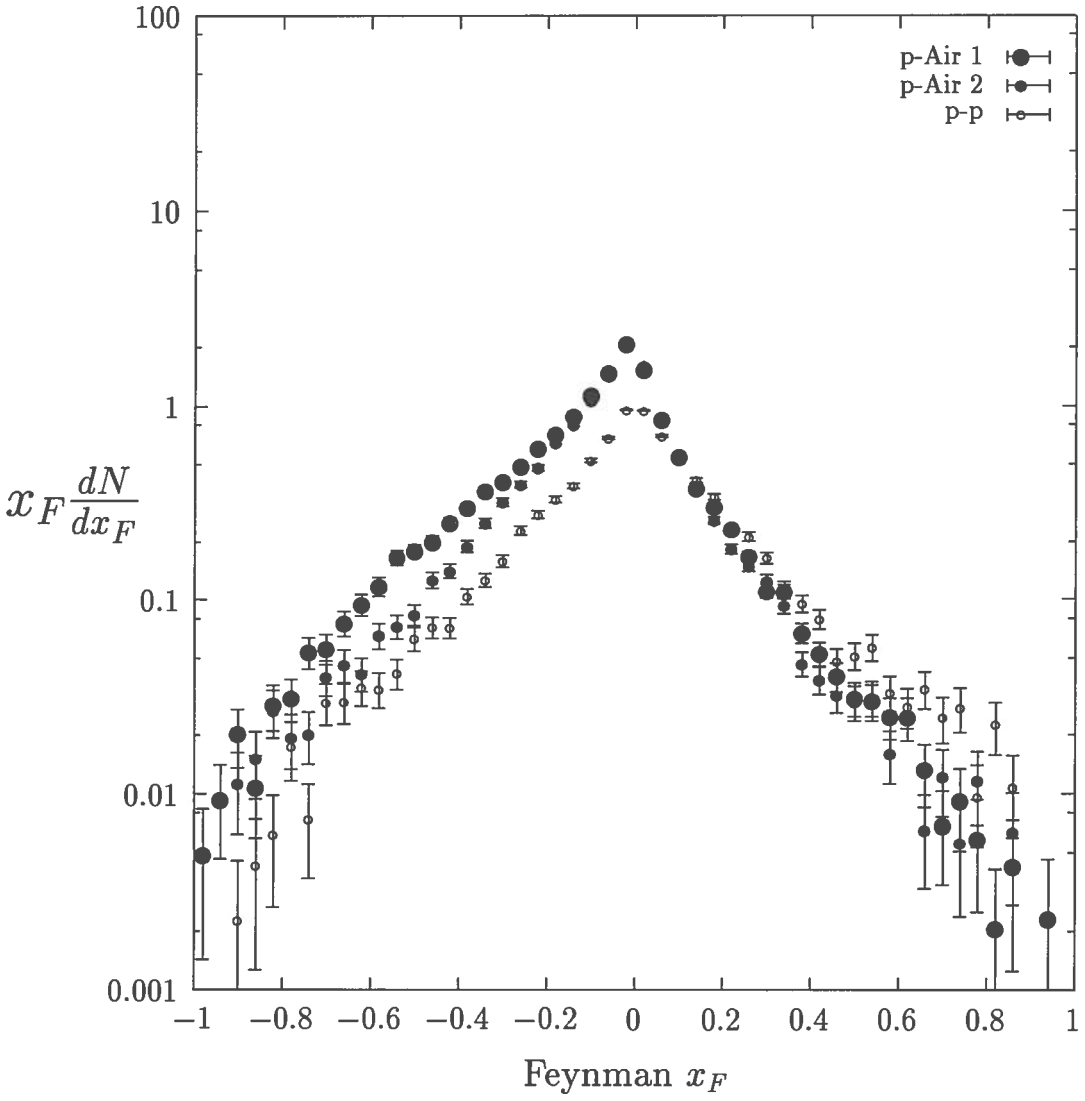

Figure 1: Feynman–x_F distribution of π^+ in p–air collisions at a lab–energy of 500 TeV. Plot 1 (large full circles) is for the full model with FZIC in the target nucleus; plot 2 (small full circles) is for the model without FZIC. The target fragmentation region is at negative Feynman–x_F, the projectile fragmentation is at positive x_F. For comparison we give also the same distribution in p–p collisions (small empty circles).

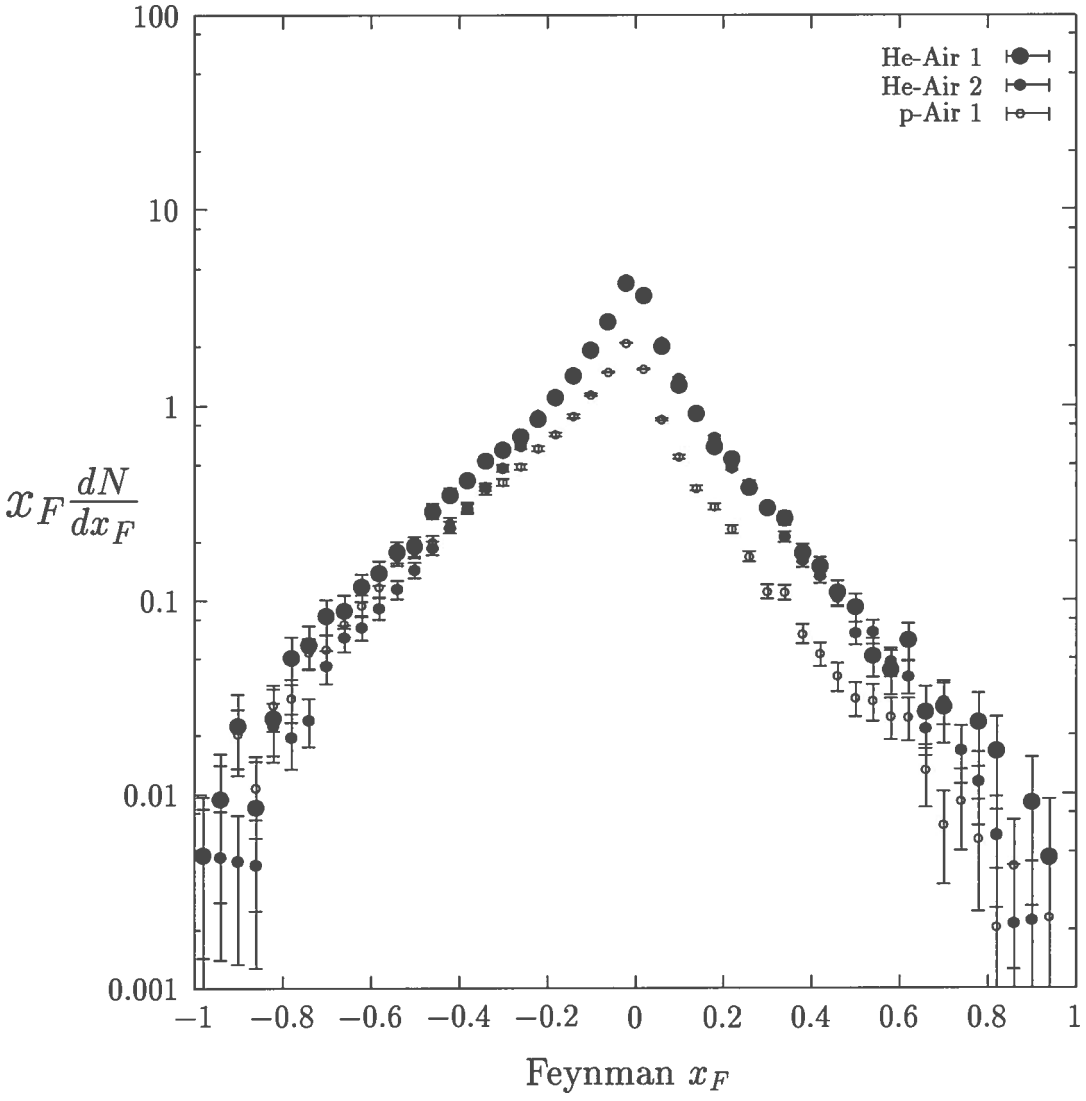

Figure 2: Feynman–x_F distribution of π^+ in He–air collisions at a lab–energy of 500 TeV per projectile nucleon. Plot 1 (large full circles) is for the full model with FZIC in the target nucleus, and projectile nucleus; plot 2 (small full circles) is for the model without FZIC. The target fragmentation region is at negative Feynman–x_F, the projectile fragmentation is at positive x_F. For comparison we give also the same distribution in p–air collisions with FZIC (small empty circles).

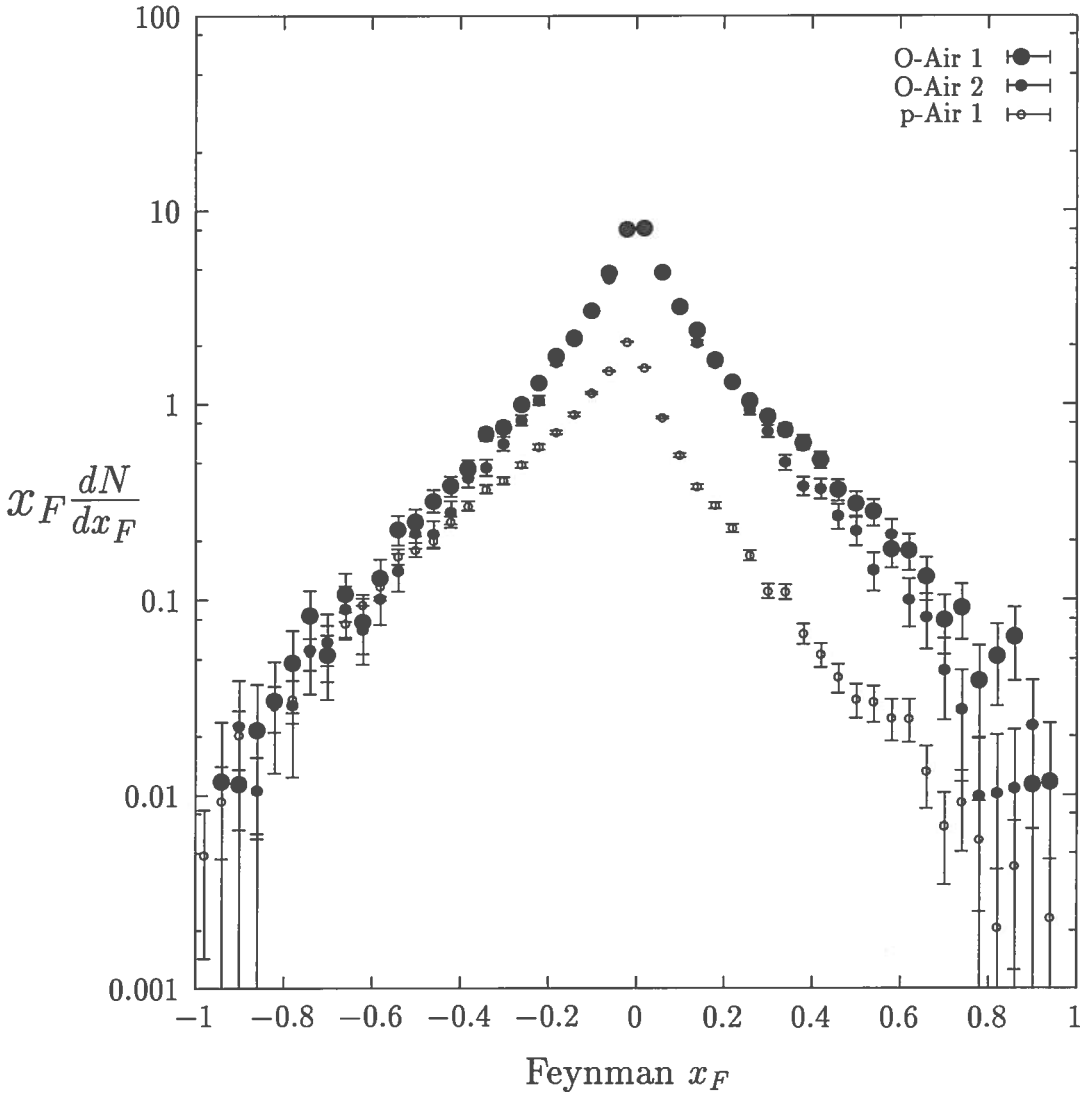

Figure 3: Feynman–x_F distribution of π^+ in O–air collisions at a lab–energy of 500 TeV per projectile nucleon. Plot 1 (large full circles) is for the full model with FZIC in the target nucleus, and projectile nucleus; plot 2 (small full circles) is for the model without FZIC. The target fragmentation region is at negative Feynman–x_F, the projectile fragmentation is at positive x_F. For comparison we give also the same distribution in p–air collisions with FZIC (small empty circles).

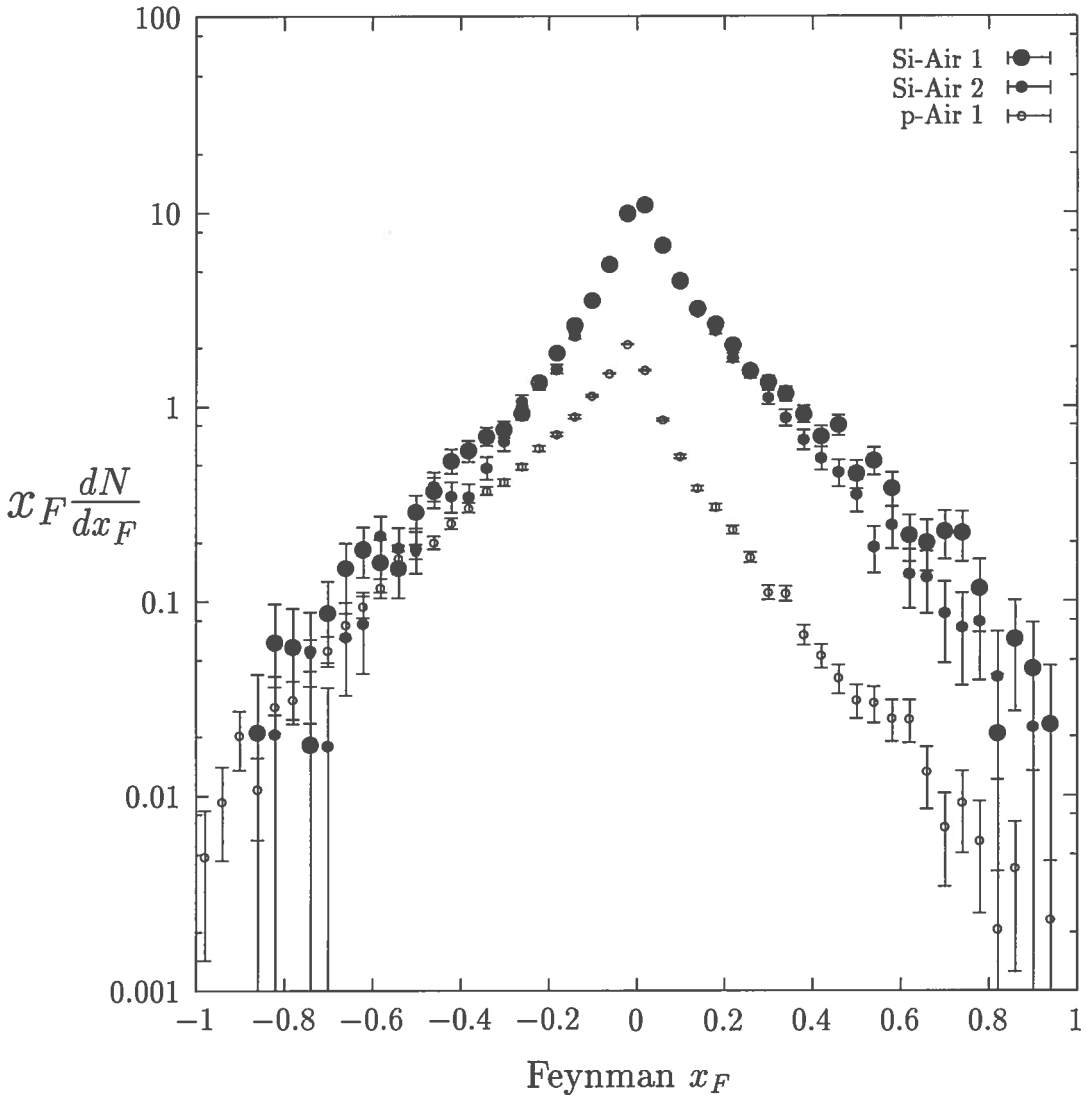

Figure 4: Feynman–x_F distribution of π^+ in Si–air collisions at a lab–energy of 500 TeV per projectile nucleon. Plot 1 (large full circles) is for the full model with FZIC in the target nucleus, and projectile nucleus; plot 2 (small full circles) is for the model without FZIC. The target fragmentation region is at negative Feynman–x_F, the projectile fragmentation is at positive x_F. For comparison we give also the same distribution in p–air collisions with FZIC (small empty circles).

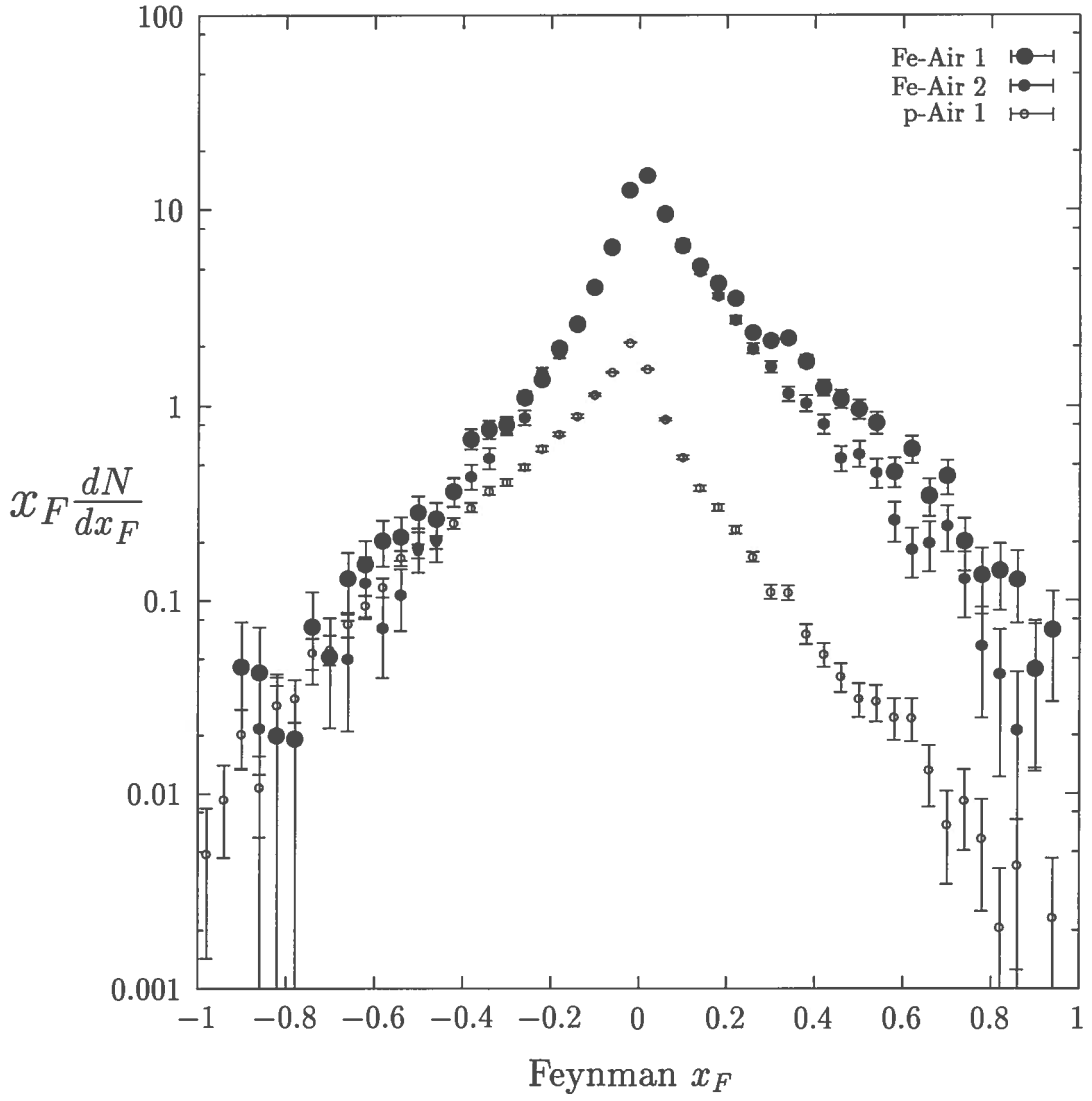

Figure 5: Feynman–x_F distribution of π^+ in Fe–air collisions at a lab–energy of 500 TeV per projectile nucleon. Plot 1 (large full circles) is for the full model with FZIC in the target nucleus, and projectile nucleus; plot 2 (small full circles) is for the model without FZIC. The target fragmentation region is at negative Feynman–x_F, the projectile fragmentation is at positive x_F. For comparison we give also the same distribution in p–air collisions with FZIC (small empty circles).